Electronic Structure of Titanium*

E. H. HYGH AND RONALD M. WELCH†
Department of Physics, University of Utah, Salt Lake City, Utah 84112
(Received 14 April 1969)

Augmented-plane-wave (APW) calculations of the electronic structure of titanium have been carried out. The resulting Fermi surface is compared to that predicted by the model of Altmann and Bradley based on cellular calculations and the APW model of Loucks for zirconium.

I. INTRODUCTION

THE present paper is a theoretical study of the electronic properties of titanium using the augmented-plane-wave (APW) method of Slater.[1] The only theoretical calculation of the Fermi surface of titanium has been carried out by Altmann and Bradley[2] (AB) who used a modified form of the cellular method suggested by Slater[3] and developed by Altmann.[4] They present results for an assumed range of valencies Ti^{+1}, Tl^{+2}, Ti^{+3}, and Ti^{+4}; their results are ambiguous to this extent. A preliminary energy-band calculation has been presented by Mattheiss[5] using the APW method, where he calculated the bands along the line of symmetry from the center of the Brillouin zone (BZ) to the K point (see Fig. 1). The work obviously is not completed, and, therefore, we have decided to calculate the energy bands and the Fermi surface using the APW method. The results will be used to predict the experimental results for de Haas–van Alphen measurements and will be compared directly with the photoemission work of Eastman.[6]

II. DETAILS OF CALCULATION

The APW method has been discussed at length in the literature and can be found elsewhere.[7] We list only those parameters and comment on only those practical aspects which are relevant to this specific calculation. Titanium is a transition metal with an atomic configuration of either $3d^34s^1$ or $3d^24s^2$, and it has the hcp crystal structure. We have chosen the more accepted atomic configuration $3d^24s^2$. The lattice constants and the APW sphere radius are listed in Table I. We employed the "muffin-tin" approximation[8] for the potential with the usual $\rho^{1/3}$ approximation taking exchange into account. The atomic-charge densities used were those of Liberman.[9] The muffin-tin potential is listed in Table II.

TABLE I. The lattice structure, the lattice constants, and the APW sphere radius for titanium.

Structure	a(a.u.)	c(a.u.)	R(a.u.)
hcp	5.5755	8.8503	2.718

The unit cell and the BZ for the hcp crystal structure are shown in Fig. 1. The basis vectors of the direct and reciprocal lattices are given by

$$\mathbf{a}_1=c\hat{k},\quad \mathbf{a}_2=\hat{\imath},\quad \mathbf{a}_3=a(-\tfrac{1}{2}\hat{\imath}+\tfrac{1}{2}\sqrt{3}\hat{\jmath}),$$

TABLE II. Muffin-tin potential for titanium inside the APW spheres. The radial distance r is in a.u. and $V(r)$ is in Ry. The constant potential region has a value of -1.939 Ry.

ln$r$	$-V(r)$	ln$r$	$-V(r)$	ln$r$	$-V(r)$
−5.40	9612.0029	−1.10	59.1402	0.15	4.8765
−5.00	6399.0328	−1.00	50.2279	0.20	4.2488
−4.60	4244.8394	−0.90	42.4468	0.25	3.6809
−4.20	2800.6691	−0.80	35.6859	0.30	3.1685
−3.80	1833.0113	−0.70	29.8591	0.35	2.7072
−3.40	1185.8834	−0.60	24.8859	0.40	2.2933
−3.20	948.4863	−0.50	20.6623	0.45	1.9233
−3.00	755.1182	−0.45	18.7935	0.50	1.5936
−2.80	597.9373	−0.40	17.5544	0.55	1.3031
−2.60	470.5298	−0.35	15.4636	0.60	1.0477
−2.40	367.6876	−0.30	13.9801	0.65	0.8262
−2.20	285.1952	−0.25	12.6061	0.70	0.6360
−2.00	219.4877	−0.20	11.3334	0.75	0.4746
−1.80	167.4140	−0.15	10.1584	0.80	0.3406
−1.60	126.3378	−0.10	9.0750	0.85	0.2306
−1.50	109.2637	−0.05	8.0782	0.90	0.1428
−1.40	94.2023	0.00	7.1653	0.95	0.0752
−1.30	80.9539	0.05	6.3297	1.00	0.0264
−1.20	69.3274	0.10	5.5687	···	···

and

$$\mathbf{b}_1=(1/c)\hat{k},\quad \mathbf{b}_2=(1/a\sqrt{3})(\sqrt{3}\hat{\imath}+\hat{\jmath}),\quad \mathbf{b}_3=(2/a\sqrt{3})\hat{\jmath}.$$

The basic dimensions of the BZ for titanium are $\Gamma A=0.354$ (a.u.)$^{-1}$, $\Gamma K=0.751$ (a.u.)$^{-1}$, $\Gamma M=0.650$ (a.u.)$^{-1}$, and $MK=0.376$ (a.u.)$^{-1}$. The reciprocal lattice vectors used in the APW expansion and designated by

$$\mathbf{K}=(n_1n_2n_3)=2\pi(n_1\mathbf{b}_1+n_2\mathbf{b}_2+n_3\mathbf{b}_3)$$

* Supported by National Science Foundation Grant No. GP-7025.
† Cooperative Research Predoctoral Fellow.
[1] J. C. Slater, Phys. Rev. **51**, 846 (1937).
[2] S. L. Altmann and C. J. Bradley, Proc. Phys. Soc. (London) **92**, 764 (1967); Phys. Rev. **135**, A1253 (1964).
[3] J. C. Slater, Phys. Rev. **45**, 794 (1934).
[4] S. L. Altmann, Proc. Roy. Soc. (London) **A244**, 141 (1958); **A244**, 153 (1958).
[5] L. F. Mattheiss, Phys. Rev. **134**, A970 (1964).
[6] D. E. Eastman, in Proceedings of the National Bureau of Standards 3rd Materials Research Symposium on Electronic Density of States, 1969, Gaithersburg, Maryland (to be published).
[7] T. L. Loucks, *Augmented Plane Wave Method* (W. A. Benjamin, Inc., New York, 1967).
[8] L. F. Mattheiss, Phys. Rev. **133**, A1399 (1964).
[9] The authors are grateful to Dr. David Liberman for making available to them the unpublished results of his atomic hfs self-consistent-field calculations for titanium.

are listed in Table III. The set of 32 vectors used gave an energy convergence good to within 0.0025 Ry on the basis of a study made at the high-symmetry points in the BZ.

The calculations were carried out over a discrete mesh which is equivalent to 3024 points in the primitive BZ. The eigenvalues were calculated at 126 general points in the 1/24 zone, 21 points on each of the six levels shown in Fig. 2. Besides these points, calculations were made at high-symmetry points and along symmetry lines.

III. RESULTS

A. Band Structure and Fermi Surface

The energy bands along symmetry directions are shown in Fig. 3. The Fermi energy was found by arranging in increasing order the 126 eigenvalues in the 1/24 zone. Since there are 4 valence electrons/atom and 2 atoms/unit cell (see Fig. 1), there are 8 electrons/cell to be accommodated. Each band can accommodate 2 electrons/cell and so we must have, on the average, four full bands. This means the lowest 504 eigenstates are

TABLE III. The 32 reciprocal-lattice vectors used in the APW expansion.

	$(2\bar{1}1)$	$(2\bar{1}0)$	(200)				
$(10\bar{1})$	$(1\bar{1}1)$	$(1\bar{1}0)$	(100)	(110)	$(11\bar{1})$	(101)	$(1\bar{2}1)$
$(00\bar{1})$	$(0\bar{1}1)$	$(0\bar{1}0)$	(000)	(010)	$(01\bar{1})$	(001)	$(0\bar{2}1)$
$(\bar{1}0\bar{1})$	$(\bar{1}\bar{1}1)$	$(\bar{1}\bar{1}0)$	$(\bar{1}00)$	$(\bar{1}10)$	$(\bar{1}\bar{1}1)$	$(\bar{1}01)$	$(\bar{1}\bar{2}1)$
$(\bar{2}0\bar{1})$	$(\bar{2}\bar{1}1)$	$(\bar{2}10)$	$(\bar{2}00)$				
			$(\bar{3}00)$				

occupied. The Fermi energy, accurate to one part in 504, is, thus, given by the highest occupied energy state. This highest occupied value was found to be 0.326 Ry. The energy of the lowest state at Γ was 0.115 Ry which gives an occupied bandwidth of 0.211 Ry. Once the Fermi energy has been found, it is a simple task to determine the Fermi surface. The $E(\mathbf{k})$ are plotted in many directions, and the $\mathbf{k}$ points at which these bands intersected the plane $E=E_F$ are found. The collection of points are then plotted and smooth curves are drawn through those points common to a given plane. Clearly, the coarse grain of the calculation implies that the shape of the surface must not be taken as the final word for titanium.

In order to show the connection of the Fermi surface elements in the third and fourth and the fifth and sixth zones, it is better to use the double-zone scheme. The double BZ is shown in Fig. 4. Also included in this figure is the 1/24 zone wedge which forms the basic domain for the energy determination. The domain in this figure labeled by n and $n+1$ are the regions in which are to be plotted the nth and $(n+1)$th energy band surfaces.

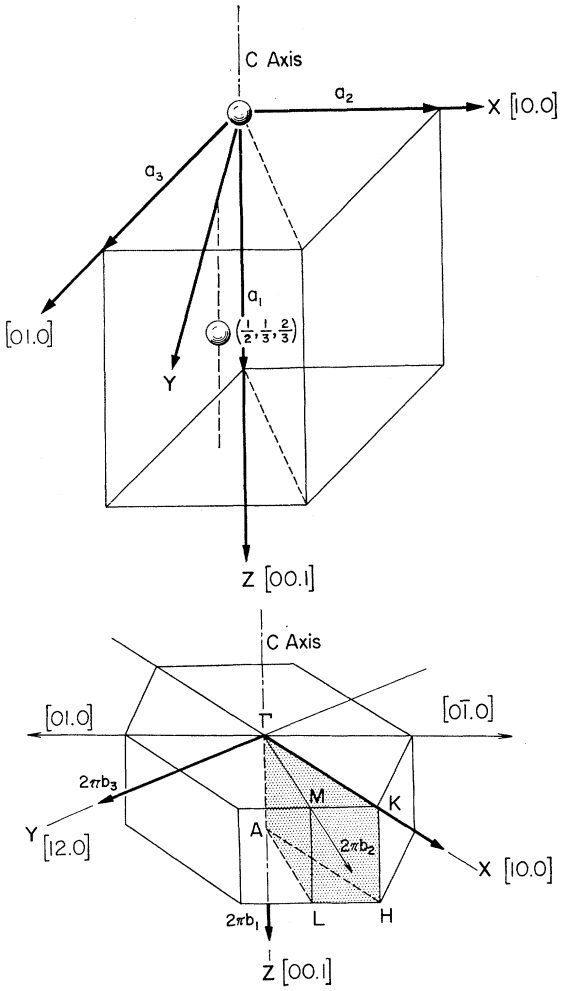

FIG. 1. The unit cell and half of the BZ for the hcp crystal structure with the 1/24 zone and crystal symmetry directions shown.

The results of our calculation show that the first and second bands are filled. The Fermi surface intersections with the 1/24 zone wedge for the third and fourth zone are shown in Fig. 5. The arrow portion of the figure gives the intersections of the Fermi surface with the double-zone-wedge symmetry planes, and the triangular portion shows the same intersection with the ALH symmetry plane. Figure 6 is the same construction for the fifth and sixth zone. The shaded parts of the figure are electron occupied. It is a simple task to construct the Fermi surface in the double-zone scheme, and these are displayed in Figs. 7 and 8. These figures are most helpful in appreciating the symmetry character of the energy surfaces.

B. Density of States

The counting scheme used to determine the Fermi energy provides a means of calculating a density-of-states histogram. This is carried out simply by counting

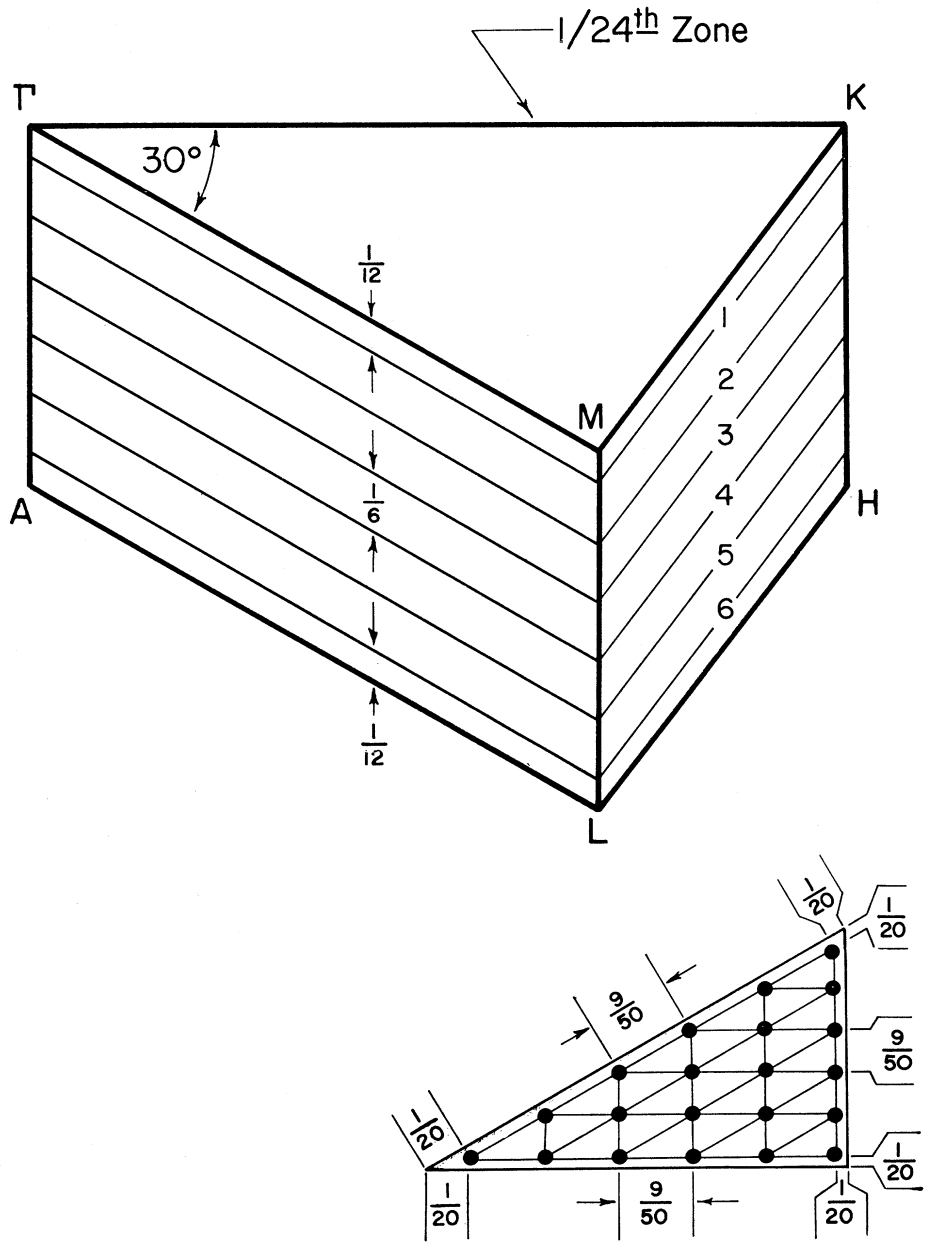

FIG. 2. The 1/24 zone showing the calculation mesh.

the number of the ordered energy eigenvalues that fall within each of a fixed set of energy intervals which covers the calculated energy range. The resulting histogram is shown in Fig. 9. The typical density-of-states curves for hcp metals is exhibited in this case. The histogram shows the two peaks due to relatively narrow d bands with the Fermi energy occurring on the high-energy side of a relatively sharp minimum. At the Fermi energy, the density of states of 28.5 electrons/atoms Ry, which gives an electronic specific-heat coefficient of $\gamma=11.81\times10^{-4}$ cal/mole deg^2. The free-electron value for this case is 1.15×10^{-4} cal/mole deg^2, and the experimental result[10] is 8.0×10^{-4} cal/mole deg^2. The d bands raise the specific heat above the free-electron value as they should. However, the theoretical result should be less than experiment because of the neglect of the lattice-electron interaction contribution. The disagreement occurs most likely because of the coarse determination of the density of states at the Fermi energy and the Fermi energy itself.

[10] J. G. Daunt, *Progress in Low Temperature Physics* (North-Holland Publishing Co., Amsterdam, 1955).

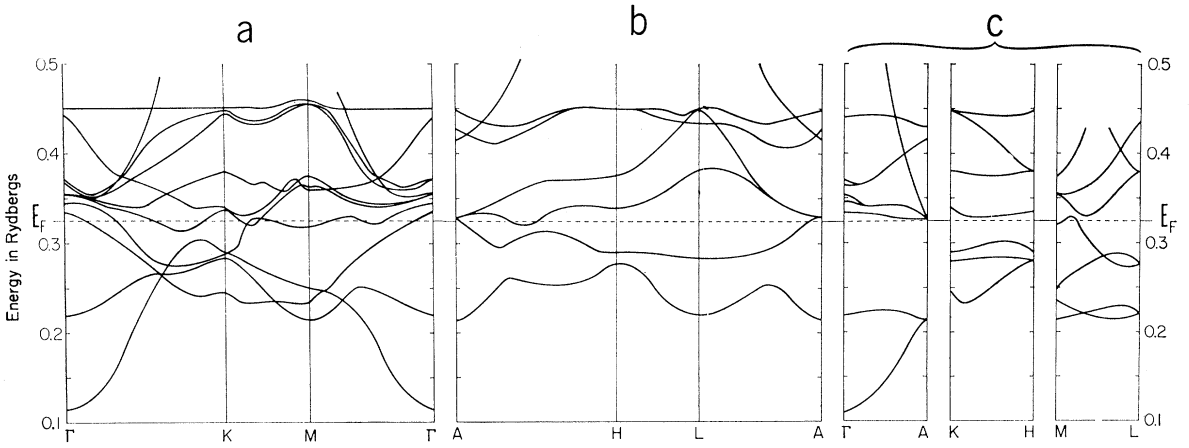

FIG. 3. The energy bands for titanium along symmetry directions. All levels in (b) are doubly degenerate.

IV. DISCUSSION

A. Comparison with Other Papers

It is helpful to contrast the results of this calculation with the cellular calculations of Ti and Zr by AB[2] and the APW calculation of Zr by Loucks.[11] The third- and fourth-zone surfaces are quite similar to the Zr calculation results of Loucks along ΓA. However, since the fourth band dips below the Fermi energy in the vicinity of the M, they are both electronlike and holelike near the symmetry point M. Also, we do not have the hole-surface structure centered on the point L as do AB. The fifth- and sixth-zone electron surfaces are quite strikingly different from the electron surfaces of Ti given by AB and Zr as presented by both Loucks and AB. The heart-shaped surface of AB and the multi-duck-billed toruslike surface of Loucks, both for Zr, become a multiply connected surface for Ti as shown in Fig. 7 and 8.

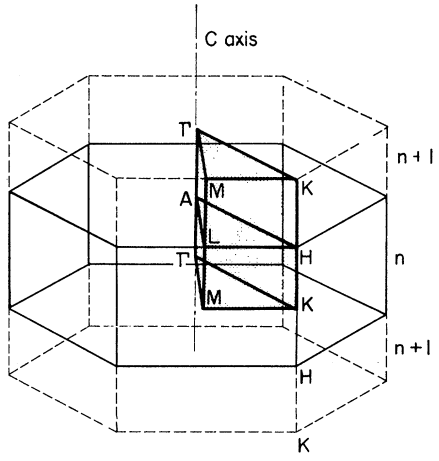

FIG. 4. The double zone. The n and $n+1$ bands are plotted in the double 1/24 wedge domain shown.

[11] T. L. Loucks, Phys. Rev. **159**, 544 (1967).

This surface is somewhat similar to the surface given by Loucks in that there is a toruslike object whose "vertical" central axis is along KH. In contrast, though, there is a second toruslike surface centered along ΓA, and the two toruslike surfaces are connected

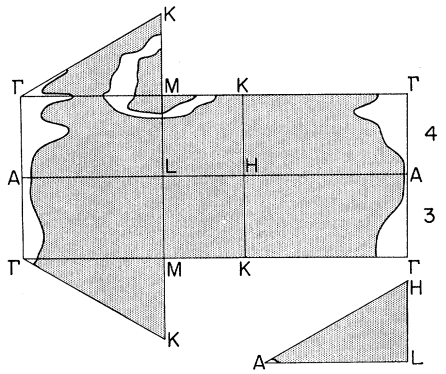

FIG. 5. Intersections of the Fermi surface with the symmetry planes of the double wedge related to the third and fourth zone.

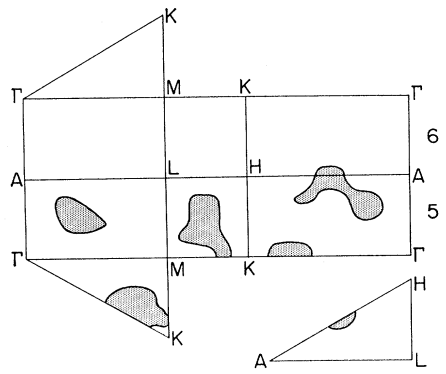

FIG. 6. Intersection of the Fermi surface with the symmetry planes of double wedge related to the fifth and sixth zone.

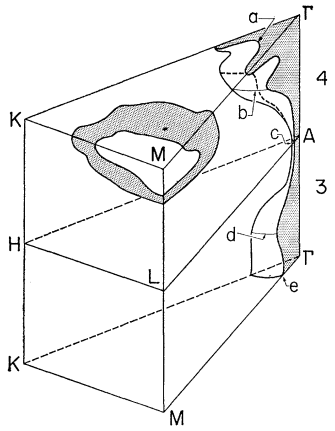

FIG. 7. The basic Fermi-surface portion for the third and fourth zone. Some of the possible orbits are labeled with lower-case roman letters. The wedge is equivalent to the basic domain and is used to elucidate the subtle features of the surface along $\Gamma A\Gamma$.

by six "horizontal" trunks, one in each separate elemental wedge.

A comparison with the cellular calculation of AB^2 for Ti shows that the gradual evolution of their model surfaces with increased valency could well lead to our results if they had increased the potential somewhat more. That is, the hole surface, about the symmetry point L, is moving toward M, and portions of surface are beginning to develop along ΓA. The manner in which their electron surfaces vary with changes in valency is more difficult to assess. It is possible that a comparison of band structure is more elucidating for this case. Our bands are similar to the Ti^{+4} structure of AB but with too many notable differences to make a comparison which is meaningful. On the other hand, Fig. 3 shows that they are almost exactly the same as the bands for Zr given by Loucks.[9] We observe the same crossing of the Fermi level by the doubly degenerate band at A, the crossing of the Fermi level by the fifth and sixth bands along AH, and the same general features along $AHLA$ for all the bands. There are notable differences however. For example, our fifth and sixth bands for Ti drop below the Fermi level along ΓK and KM, and our third and fourth bands rise above the Fermi level along KM and $M\Gamma$. A fourth band crossing, which is absent for Zr, also occurs along ML close to M. There is a degeneracy along HK which the Loucks's calculation does not exhibit. Clearly, it is this set of rather innocent-looking differences in the structure which gives rise to the dramatic difference in both the hole and the electron Fermi surfaces for Ti when compared to Zr. That is, we find a closed-electron surface and a closed-hole surface both in the fourth zone centered around M, and two open-hole surfaces in the fifth zone, one centered on K and the other along ΓA centered at about 0.6 ΓA. These latter hole surfaces are actually the inner portions of the two toroidal objects described above.

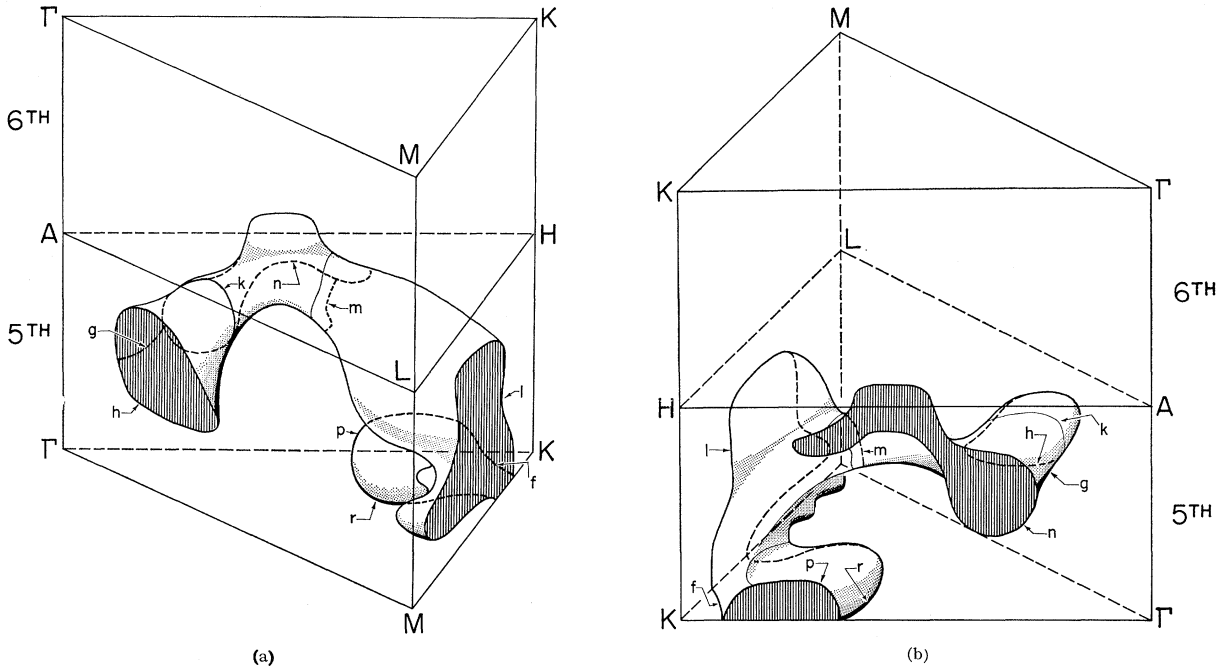

FIG. 8. The basic Fermi-surface portion for the fifth and sixth zone. Some of the possible orbits are labeled with lower-case roman letters. Figure 8(b) is a back view of Fig. 8(a).

B. de Haas–van Alphen Periods

Possible orbits of the electrons will be discussed, since some extremal areas can be suggested from the results of our Fermi surface calculation. Since there are no experimental data available (which are a measure of the Fermi surface of titanium), the following discussion is clearly speculative.

The third- and fourth-zone hole surface along $\Gamma A\Gamma$ is essentially the same as the Loucks results for Zr before his suggested modification. This surface clearly gives five extremal cross sections normal to the c axis or [00.1] direction. This dot notation $[a_1a_2\cdot c]$ is equivalent to the Miller index notation $[a_1a_2a_3c]$. In this case, the redundant coordinate d_3 is omitted (see Fig. 1). Portions of the corresponding orbits are labeled a, b, c, d, and e in Fig. 7. The periods, in units of 10^{-8} G^{-1}, are given in Table IV. The five easily observable periods associated with the five possible orbits of this surface will vary with angle and eventually will die off for angles above approximately 30°.

In contrast to the results for Zr, the fourth-zone hole and electron surfaces at symmetry point M give two sets of periods which are fairly constant for the magnetic field along the directions [00.1], [10.0], and [1$\bar{1}$.0] (i.e., ΓA, ΓK, and ΓM, respectively). The sections (see Fig. 5 or 7) centered on M give the following periods for holes:

Direction	Period (10^{-8} G^{-1})
[00.1]	3.1
[10.0]	6.6
[1$\bar{1}$.0]	3.8;

and the following periods for electrons:

Direction	Period (10^{-8} G^{-1})
[00.1]	4.1
[10.0]	12.0
[1$\bar{1}$.0]	8.7.

These surfaces both have rather large periods which change rapidly with angular variation about the [10.0] direction. Thus, it would require some care in order to measure them.

Finally, in Table IV, are listed periods for orbits associated with the multiply-connected fifth-zone electron surface. Portions of these orbits are labeled as shown in Figs. 7 and 8, and the diagrams show that most of these orbits are highly sensitive to the topography of the Fermi surface. Also, many orbits have periods which are very large and, thus, might well require fairly pure single crystals in order to measure them. Orbits f and g are the hole orbits associated with the toroidal objects, and they are extremely sensitive to both field orientation and topography. Consequently, they are extremely unlikely candidates for observation. The same is true for the electron orbits labeled n and r.

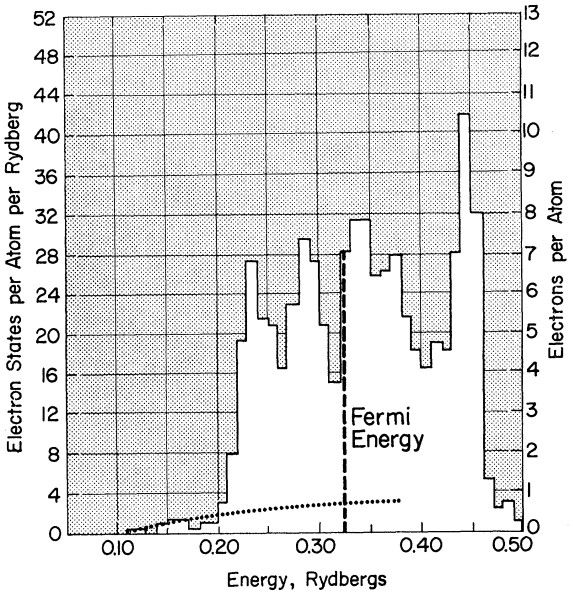

FIG. 9. Histogram of the density of states with the Fermi energy indicated by a dashed line. The dotted curve is from the free-electron model.

On the other hand, orbits h and k occur where the surface has small curvature along the [10.0] direction. Thus, they are very likely to be observed only for a limited range of angles about the [10.0] direction. The same is true for orbits l, m, and p for the [1$\bar{1}$.0] direction of the magnetic field. Orbit m has a very long period which makes it an excellent candidate for low-field study, as long as one has pure enough crystals available.

C. Photoemission Studies

A recent photoemission study[5] of titanium shows that the d bandwidth of titanium at half-maximum is 2.0 eV. The present paper gives a somewhat coarse density of

TABLE IV. Periods of the orbits labeled in Figs. 7 and 8.

Direction	Orbit		Period (10^{-8}G^{-1})
[00.1]	Third and	a(hole)	3.6
	fourth bands	b(hole)	1.8
		c(hole)	9.7
		d(hole)	3.8
		e(hole)	7.0
	Fifth and	f(hole)	15.0
	sixth bands	g(hole)	4.1
		r(elec.)	1.3
[10.0]	Fifth and	h(elec.)	17.0
	sixth bands	k(elec.)	22.0
[1$\bar{1}$.0]	Fifth and	l(elec.)	3.3
	sixth bands	m(elec.)	76.0
	n(elec.)	n(elec.)	9.4
		p(elec.)	17.0

states histogram (see Fig. 9) which has a width at half-maximum of ~0.01 Ry or ~1.4 eV. This is narrower than the experimentally resolved structure and is in much better agreement with Eastman's work than suggested by his comparison with an extrapolated value using the zirconium results of Loucks.

V. CONCLUSIONS

The fact that little experimental data are available dictated the nature of this calculation. No attempt was made to include the spin orbit or other relativistic effects, and no effort was made to guarantee self-consistency. It is almost certainly true that some of the more subtle features of the Fermi surface will have to be modified when experimental data become available. It is hoped that this calculation will lead to an interest in the study of titanium, since it appears to be an excellent candidate for displaying all the general features exhibited by hcp metals.

ACKNOWLEDGMENTS

The authors are pleased to acknowledge the helpful comments of Larry J. Page in modifying the APW computer program for use on the Univac 1108 computer. One of us (E.H.H.) is pleased to thank Dr. Terry L. Loucks for his helpful discussion concerning the APW method and Dr. Conrad Miziumski for a stimulating discussion concerning the de Haas–van Alphen effect. A special note of thanks goes to Dr. David A. Liberman for providing the results of his atomic hfs self-consistent-field calculations for titanium which were in a form amenable to the APW method.

PHYSICAL REVIEW B VOLUME 1, NUMBER 6 15 MARCH 1970

Lattice Dynamics of Yttrium at 295 K*

S. K. SINHA, T. O. BRUN, L. D. MUHLESTEIN,† AND J. SAKURAI‡
Institute for Atomic Research and Department of Physics, Iowa State University, Ames, Iowa 50010
(Received 5 September 1969)

Phonon-dispersion curves along the [10$\bar{1}$0], [11$\bar{2}$0], and [0001] symmetry directions of the hcp metal yttrium have been measured by inelastic neutron scattering using the triple-axis neutron spectrometer at the Ames Laboratory Research Reactor. The dispersion curves are not strikingly different from those of other hcp metals with a similar c/a ratio. A careful search has been made for Kohn-type anomalies, and evidence for two such anomalies has been obtained. A modified axially symmetric force-constant model has been used to fit the phonon frequencies, and it has been found that although forces acting normally to the basal plane are not large beyond first neighbors, forces acting parallel to the basal plane are long-ranged, and interactions up to at least sixth neighbors have to be taken into account. The fitting has been done in a linear manner using Fourier analyses of the dispersion curves and other linear constraints such as the elastic constants. A frequency-distribution function has been calculated and used to calculate the specific heat and anisotropic Debye-Waller factor. Good agreement is obtained on comparison with the experimental data.

I. INTRODUCTION

OVER the last few years, neutron-scattering measurements of the phonon-dispersion curves of several hcp metals have been reported, including magnesium,[1,2] beryllium,[3,4] zinc,[5] and holmium.[6] Of these, the first three are generally regarded as free-electron–like in electronic structure. The measurements reported in this paper were originally undertaken to obtain detailed information about the lattice dynamics of the rare-earth–type metals, in view of the current interest in the properties of these metals and the considerable theoretical and experimental work being carried out in this area. Yttrium is actually to be regarded as a prototype rare-earth metal since it does not possess any f shells. However, its electronic structure[7] is very similar to the rare earths, as far as the conduction electrons are concerned, and like them it crystallizes in a hcp structure with a c/a ratio close to the ideal. The lattice constants for yttrium at room temperature are $a=3.6474$ Å, $c=5.7306$ Å, and $c/a=1.5711$. Information about the phonon spectra of the rare-earth–type metals has since been obtained by the Brookhaven group on holmium,[6] by the Oak Ridge group on holmium

* Work performed in part in the Ames Laboratory of the U. S. Atomic Energy Commission. Contribution No. 2617.
† Present address: Department of Physics, University of Missouri, Columbia, Mo. 65201.
‡ Present address: Faculty of Science, University of Hiroshima, Hiroshima, Japan.
[1] P. K. Iyengar, G. Venkataraman, P. R. Vijayaraghavan, and A. P. Roy, in *Inelastic Scattering of Neutrons in Solids and Liquids* (International Atomic Energy Agency, Vienna, 1965), Vol. I, p. 153.
[2] G. L. Squires, Proc. Phys. Soc. (London) **88**, 919 (1966); G. L. Squires and R. Pynn, in *Neutron Inelastic Scattering* (International Atomic Energy Agency, Vienna, 1968), Vol. I, p. 215.
[3] R. E. Schmunk, R. M. Brugger, P. D. Randolph, and K. A. Strong, Phys. Rev. **128**, 562 (1962).
[4] R. E. Schmunk, Phys. Rev. **149**, 450 (1966).
[5] G. Borgonovi, G. Caglioti, and J. J. Antel, Phys. Rev. **132**, 683 (1963).
[6] J. A. Leake, V. J. Minckiewicz, and G. Shirane, Solid State Commun. **7**, 535 (1969).
[7] T. L. Loucks, Phys. Rev. **144**, 504 (1966).